

Preparation of tin and tin sulfide alloy on carbons and graphene via chemical method for use as anodes in lithium-ion batteries

Thitima Waket^a, Thapanee Sarakonsri^{a,b,*}, Katerina E. Aifantis^{c,d} and Stephen A. Hackney^e

^aDepartment of Chemistry and Center for Innovation in Chemistry (PERCH-CIC), Faculty of Science, Chiang Mai University, Chiang Mai 50200, Thailand

^bMaterials Science Research Center, Faculty of Science, Chiang Mai University, Chiang Mai 50200, Thailand

^cLab of Mechanics and Materials, Aristotle University, Thessaloniki 54124, Greece

^dCivil Engineering-Engineering Mechanics, University of Arizona, Tucson, AZ 85721, USA

^eMaterials Science and Engineering, Michigan Technological University, Houghton, MI 49931, USA

Both tin (Sn) and sulfur (S) can act as hosts for lithium-ions and, therefore, Sn/C and SnS/C nanocomposites, prepared by the solution method, have the potential to be used as anodes in next-generation Li-ion batteries. One of the key factors in the design of promising anodes is the ability of their microstructure to accommodate the Li-insertion and de-insertion; hence, in the present study, various carbon types were employed, and the metal volume fractions (S and Sn) were varied in order to determine the most promising microstructures. Particularly, the types of carbons, which were considered in this study, were artificial graphite (AG), mesocarbonmicrobeads (MCMB), and graphene (GC). To prepare Sn/graphene composites, the amount of Sn was made to vary between 10 wt.% and 20 wt.%. As for the SnS/C materials, the Sn and S ratios were 10 : 10 and 20 : 20, and the types of carbon used were MCMB and AG. X-ray diffraction showed that Sn and SnS phases develop within graphite, and scanning electron microscopy revealed that these phases disperse well in graphite. Furthermore, transmission electron microscopy allowed for a better observation of the nanometer dimensions of the particle size in all the samples.

Key words: Lithium batteries, Anode materials, Composites, Tin And tin sulfide.

Introduction

Lithium-ion batteries are widely used as power sources for portable devices such as cellular phones, laptop computers, and digital cameras. Their performance, however, is limited by the low reversible specific capacity (372 mAh/g) achieved by commercial graphitic anodes [1]. Various metal composites, metal oxides, and metal sulfides have been studied extensively as possible alternatives to carbonaceous anode materials because of their high capacities upon their reaction with Li [2-7]. For example, S, Sn, and Sb have capacities of 1672 mAh/g, 996 mAh/g, and 660 mAh/g, respectively, which are much higher than the capacities provided by commercial graphite [6-10]. The high capacities of these metals, however, are accompanied by the large volume expansions, and subsequent contractions, which occur during Li-insertion and de-insertion. These volume changes induce mechanical stresses, which result in the disintegration of the electrode and reduce the electrode lifetime.

In order to minimize these volume expansions, a

common practice that battery developers have resorted to is to embed or attach the Li-active metals on carbon. The carbon matrix acts as a protecting shell and provides enough free volume to accommodate the expansion-contraction of metal particles, assuring electrochemical cycling stability. Furthermore, the carbon matrixes provide the electron transport pathways due to the high electronic conductivity of the carbonaceous materials. Hence, it is evident that Sn/C, S/C, and SnS/C composites have the potential to be promising anodes for rechargeable Li-ion batteries. Several forms of carbon supports have been attempted, such as particles, nanotubes, natural graphite, and graphene [11-15]. Graphene (a single layer of carbon, with a honeycomb structure), in particular, has attracted significant attention over the past few years. Its large surface area and high strength offer promising applications in composites, supercapacitors, nanoelectronics, and electrodes [16-17]. Particularly, a recent mechanics study on the damage of nanocomposites during Li-insertion predicted that graphene allows for the best mechanical stability [18]. In the present article, a new fabrication method is presented for producing Sn/C, and SnS/C nanocomposites using a chemical method. In order to obtain the most optimum microstructure, various types of carbon (artificial graphite, mesocarbonmicrobead, and graphene) were employed, and the Sn wt.% and S wt.% were varied. In

*Corresponding author:
Tel : +66-53941907
Fax: +66-53892277
E-mail: tsarakonsri@gmail.com

the future, lithium-ion batteries will undergo improvement in safety, energy densities, capacity retention, and many more features. This will make it possible to obtain high-quality performance anode materials for applications in pieces of equipment such as electric vehicles and future mobile devices. Making the production process extremely economic and using cheaper material are of utmost importance. At the same time, physical and chemical modifications of the electrode materials with a view to improving the electrochemical performance design in the structure, and composition for minimizing the volume changes in the electrode are necessary.

Experiment Details

Preparation of Sn/C composite

The preparation procedure was carried out by using N_2 gas to bubble the ethylene glycol solvent (99.9%, J.T. Baker). Then, $SnCl_2 \cdot 2H_2O$ (99.9%, Fluka) was added, while the solution was stirred until it completely dissolved. Next, the carbon precursor was added to the solution, which was then sonicated for 2 hours. After sonication, $NaBH_4$ (> 96%, Merck) was used to reduce the Sn^{2+} ions contained in the solution, and the reaction was stopped after 15 minutes. After that, it was sonicated again, for 2 hours. The precipitate was collected by centrifugation and washed with ethanol (99.9%, MERCK). Finally, the product was dried at 70 °C for 2 hours to obtain the final powder. The Sn content used was 10 wt.% and 20 wt.% on each carbon type.

Preparation of SnS/C composite

The wt.% ratios of Sn and S were 10 : 10 and 20 : 20, while the types of carbon were MCMB and AG. In the experimental process, $SnCl_2 \cdot 2H_2O$ (99.9%, Fluka) and NH_2CSNH_2 (99.0%, Merck) were used as the precursors, and they were refluxed in ethylene glycol (99.9%, J.T. Baker) at 200 °C for 8 hours. The precipitate obtained was collected by centrifugation and washed using ethanol. Finally, the product was dried at 70 °C for 2 hours to obtain the product powder.

All the prepared samples were characterized using X-ray diffraction (XRD) for phase identification by Bruker AXS diffractometer D8 Advance with a scanning rate of 0.04 °/s in the 2θ range between 10 ° and 80 ° (for the Sn/C and SnS/C composites) and 20 ° and 80 ° (for the S/C composite). The morphology of all the samples was determined using scanning electron microscopy (SEM, JEOL JSM-5910LV and SEM, JEOL JEM-6335FE) and transmission electron microscopy techniques (TEM, JEOL JEM-2010). Energy dispersive spectroscopy (EDS, INCA-The Microanalysis Suite Issue 16) was used to identify the element type and the percentage weight.

Results and Discussion

The XRD patterns of the Sn/graphene sample where

the wt.% of Sn was fixed at 10 wt.% and 20 wt.% are shown in Figure 1 and Figure 2, respectively. The XRD results reveal that sample (a) and sample (b) of both Figure 1 and Figure 2 contained the phases which corresponded to carbon, which has a hexagonal structure (JCPDS card no. 41-1487), and Sn, which has a tetragonal structure (JCPDS card no. 4-673), while sample (c) of both Figure 1 and Figure 2 contained the phases which corresponded to carbon, which has a rhombohedral structure (JCPDS card no. 26-1079), and Sn (JCPDS card no. 4-673). The differences in the diffraction patterns of carbon originated from the differences in the carbon crystal structures. Carbon AG and MCMB are types of graphite, which are layered materials that are formed by a number of two-dimensional graphene crystals weakly coupled together, while graphene is a single-atom-thick sheet (sp^2 -bonded carbon atoms) of a honeycomb carbon lattice [18].

The formation mechanisms of the Sn/C composites can be explained in a manner similar to the SnSb/C composites, which were studied by Adpakpang et al. [7]. The production of the Sn phase on carbon can occur under the reducing process of sodium borohydride ($NaBH_4$) when ethylene glycol is used as the solvent. The Sn^{2+} ions in the solution take electrons

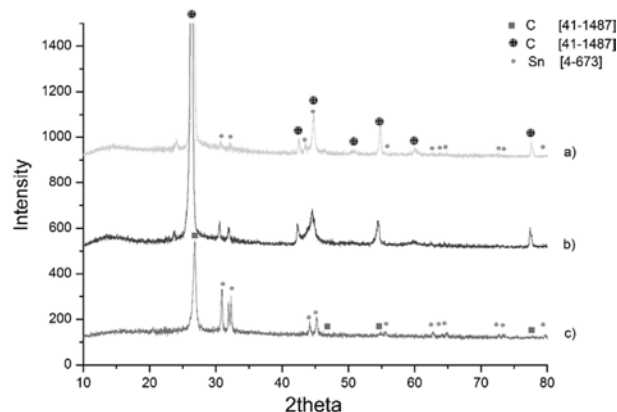


Fig. 1. The XRD patterns of (a) 10 Sn/AG composite, (b) 10 Sn/MCMB composite, and (c) 10 Sn/GC composite.

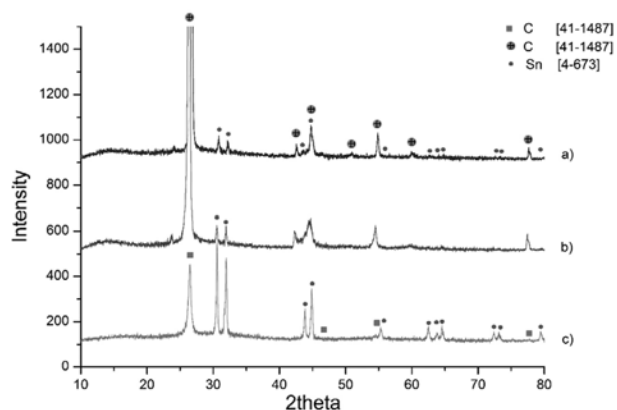
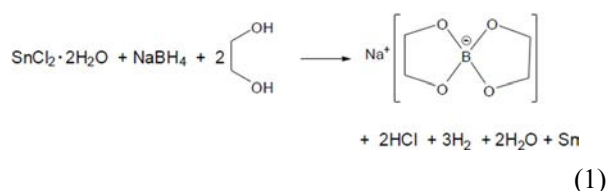


Fig. 2. The XRD patterns of (a) 20 Sn/AG composite, (b) 20 Sn/MCMB composite, and (c) 20 Sn/GC composite.

Table 1. Measured full width at half maximum (B_r), 2θ , and calculated particle size (L) of graphite and graphene from XRD.

Sample type	2θ ($^\circ$)	B_r ($\times 10^{-3}$)	L (nm)
Graphite (10 Sn/MCMB)	26.382	4.99	238.58
	42.223	7.36	
	44.393	15.90	
Graphene (10 Sn/GC)	54.543	10.00	7.44
	26.603	20.00	

from NaBH_4 , and form Sn pure phase, as indicated in Reaction (1). Hence, NaBH_4 serves as the reducing agent ($E^0 = -1.24$ V) in this reaction. It donates electrons to Sn^{2+} (Sn^{2+}/Sn , $E^0 = -0.14$ V) cations to form Sn on the carbon surface [7].



From Figure 1b and Figure 2b, it can be seen that the carbon peaks at $2\theta = 44.39^\circ$ and $2\theta = 54.54^\circ$ disappear for graphene. The XRD peak intensity can also be used to calculate the average crystallite size of carbon. The differences in the average carbon grain size can affect the Sn particle size, and the amount of Sn on carbon materials can be predicted by using the Scherrer formula in Equations (2)-(3), where λ is the wavelength of the X-rays (0.15406 nm), θ is the Bragg angle, L is the average crystallite size, B is the full width at half maximum, and k is a constant (0.94) [19].

$$B_{\text{crystallite}} = \frac{k\lambda}{L \cos \theta} \quad (2)$$

$$B_r \cos \theta = \frac{k\lambda}{L} + \eta \sin \theta \quad (3)$$

The measured full width at half maximum (B) and 2θ of graphene from the XRD patterns are listed in Table 1. The average carbon particle size (L) can be obtained from Equation (2) for graphene and Equation (3) for graphite because there are several XRD peaks that appeared for graphite but only one for graphene. Therefore, Equation (3) was applied for graphite for which a plot needs to be made to get the result, while Equation (2) was used for graphene, and the values can be directly substituted in it to obtain the solution. Figure 3 shows a graphite plot between $B_r \cos \theta$ on the y -axis and $\sin \theta$ on the x -axis, where $\sin \theta$ is obtained directly from Equation (3). The crystallite size is calculated from the y -axis intersection, which is equal to $k\lambda/L$ in Equation (3). Then, L is calculated to be 238.58 nm for graphite. For graphene, L was calculated directly from Equation (2), and was found to be equal

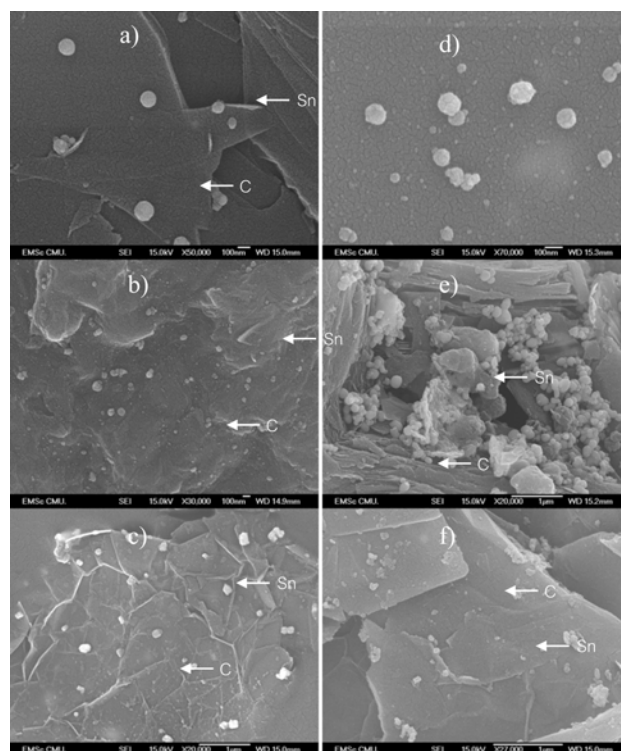


Fig. 3. The SEM images of (a) 10 Sn/AG composite, (b) 10 Sn/MCMB composite, (c) 10 Sn/GC composite, (d) 20 Sn/AG composite, (e) 20 Sn/MCMB composite, and (f) 20 Sn/GC composite.

to 7.44 nm. It was observed that the average grain size of graphene is much smaller than that of the artificial graphite.

Figure 3 shows the SEM images for the Sn/AG, Sn/MCMB, and Sn/GC samples with 10 wt.% and 20 wt.% of Sn. The figure also indicates that all the metal particles are spherical in shape and well dispersed on the carbon surface. The particle sizes for the 10 wt.% Sn were 51.53 nm on GC, 86.22 nm on AG, and 86.78 nm on MCMB. Similarly, for the 20 wt.% samples, the particle sizes of Sn were 51.75 nm on GC, 87.92 nm on AG, and 88.71 nm on MCMB. Although the average Sn particle sizes on both the materials are similar, the standard deviation of 10 wt.% Sn on carbon is better than the standard deviation of 20 wt.% Sn on carbon — a phenomenon that can significantly improve the cycling performance of anodes [20]. At the same time, the particle size of Sn on graphene is smaller than the particle size of Sn on both the types of graphite. The particle size histograms of 10 wt.% Sn on carbon and 20 wt.% Sn on carbon are illustrated in Figure 4. It is interesting to note that the particle size is related to the surface area of each carbon matrix, as shown in Table 2. Graphene provided an abundant area for the Sn particles to deposit on, and therefore small Sn particles were well dispersed onto its surface. On the other hand, using AG and MCMB, which have less surface area than graphene, resulted in the formation of larger

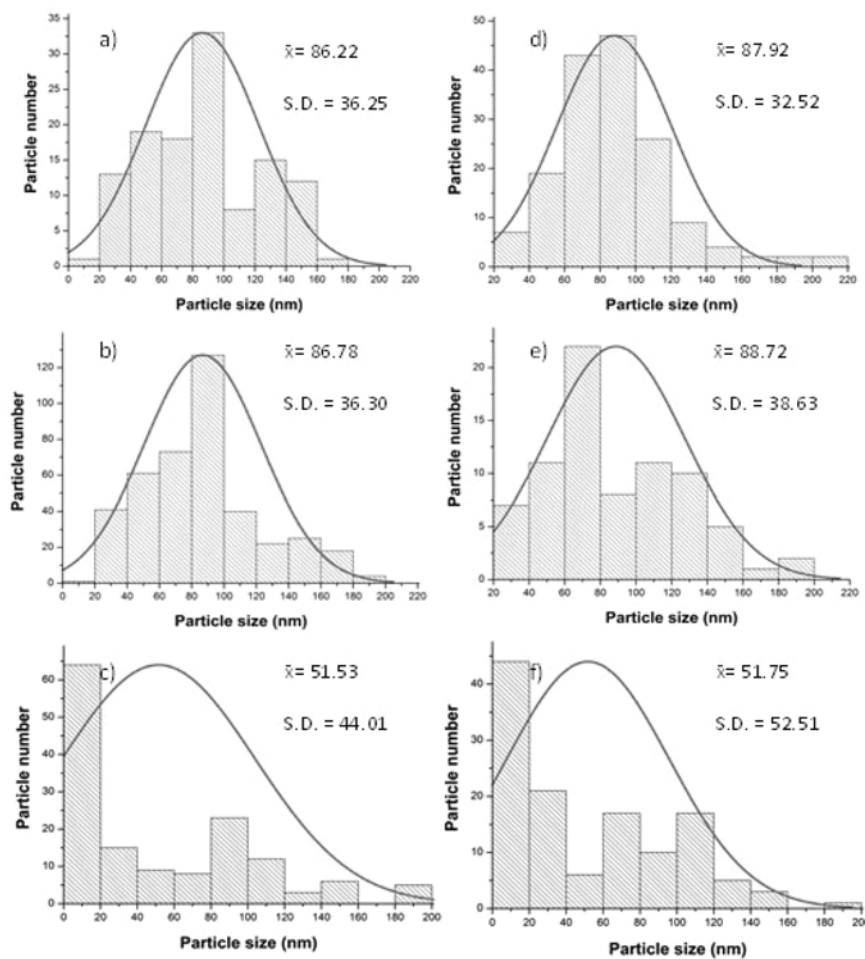


Fig. 4. The particle size histograms of (a) 10%Sn/GC composite and (b) 20%Sn/GC composite.

Table 2. Surface area of carbon.

Type of Carbon	Surface area ($\text{m}^2 \cdot \text{g}^{-1}$)
Mesocarbon-Microbead (MCMB)	1.67
Artificial Graphite (AG)	2.14
Graphene	1256

particles [7, 18].

The amount of elements contained in each sample was measured using energy dispersive spectroscopy (EDS). In order to get the figures to be representatives

of the elemental amount, the measurement was performed in five random areas in each sample. The elemental amounts for all the preparative samples are presented in Table 3. Stoichiometric ratios indicate that there are slight elemental amounts in all the composites. It should be noted that this cannot be described as the actual amount of the sample.

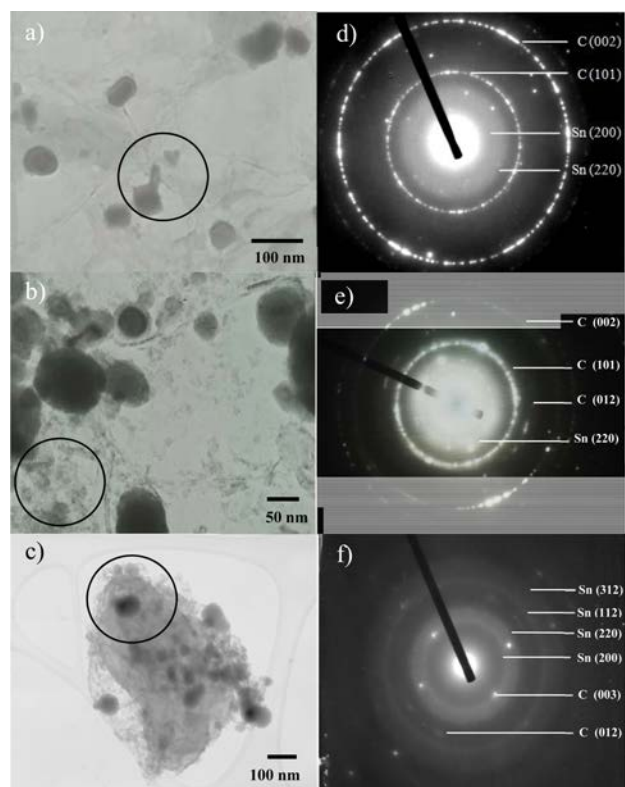
For obtaining information regarding the composition of the Sn/C composites, thermogravimetric analysis (TGA) was carried out. Table 4 presents the TGA analysis of the 10 wt.% Sn/GC composite and the 20 wt.% Sn/GC composite. The large internal surface area of carbon has strong attractive forces that attract

Table 3. Elemental measurement by EDS technique of all samples.

No.	Ratio of Elements	Type of Carbon	Particle Size (nm)	%Elements (%wt)		
				Sn	C	S
1	10 Sn : 90GC	Graphene (from China)	51.53	10.77	89.23	–
2	20 Sn : 80GC	Graphene (from China)	51.75	18.15	81.85	–
3	10 Sn : 10 S : 80AG	Artificial Graphite	254.33	23.21	73.74	3.05
4	10 Sn : 10 S : 80MCMB	Mesocarbon Microbead	494.35	25.6	69.78	4.27
5	20 Sn : 20 S : 60AG	Artificial Graphite	411.34	26.23	65.89	7.88
6	20 Sn : 20 S : 60MCMB	Mesocarbon Microbead	559.91	33.68	56.84	9.48

Table 4. TGA results of Sn/C composites.

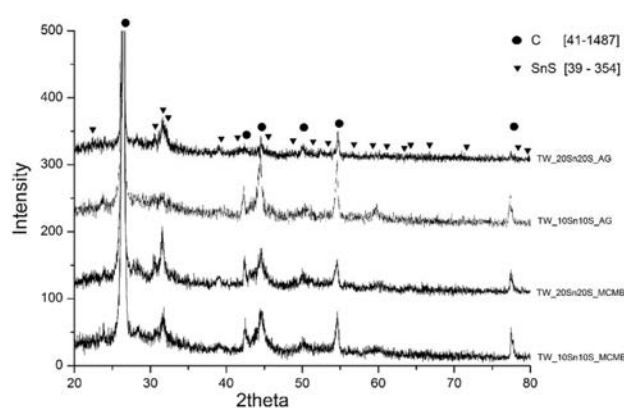
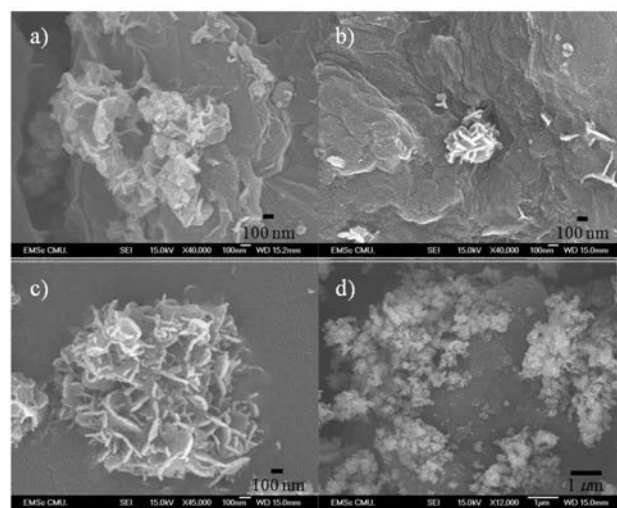
Sample	Percentage of Sn
10 wt.%Sn/GC	9.05
20 wt.%Sn/GC	19.76

**Fig. 5.** The TEM images of (a) 20 Sn/AG composite, (b) 20 Sn/MCMB composite, and (c) 20 Sn/GC composite, and the SAD patterns of (d) Sn/AG, (e) Sn/MCMB, and (f) Sn/GC.

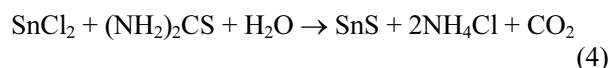
other molecules.

Figure 5 shows the TEM images and the selected area diffraction (SAD) patterns of the 20% Sn-C composites. The particles of Sn are spherical in shape. The SAD patterns indicate the bright rings as the carbon phase and the diffuse rings as the Sn particles. The SAD pattern in Figure 5(d) shows spot-ring patterns as a result of the large particle size of carbon. This result is consistent with the TEM image seen in Figure 5(a). The SAD pattern in Figure 5(e) shows non-continuous ring patterns because this sample contained carbon particles in different sizes. This result is consistent with the TEM image seen in Figure 5(b). Finally, the SAD pattern in Figure 5(f) shows bright spots patterns, which are a result of the large particle size of carbon, and the diffuse rings and the less bright ring patterns are a result of the small particle size of Sn. This result is consistent with the TEM image seen in Figure 5(e). These TEM results are in good agreement with the XRD and SEM results.

As for the SnS/C samples, Figure 6 shows the XRD patterns for which the Sn : S ratio was 10 : 10 on AG

**Fig. 6.** The XRD patterns of (a) 20 Sn20 S/AG composite, (b) 10 Sn10 S/AG composite, (c) 20 Sn20 S/MCMB composite, and (d) 10 Sn10 S/MCMB composite.**Fig. 7.** The SEM images of (a) 10 Sn10 S/AG composite, (b) 10 Sn10 S/MCMB composite, (c) 20 Sn20 S/AG composite, and (d) 20 Sn20 S/MCMB composite.

(Figure 6b) and MCMB (Figure 6d). At the same time, the ratio of Sn and S is 20 : 20 on AG (Figure 6a) and MCMB (Figure 6c). The XRD results show that this sample contained the phases which corresponded to carbon (JCPDS card no. 41-1487) and SnS (JCPDS card no. 39-354). The formation of the SnS phase can be explained using Reaction (4).



The SEM images of the 10 wt.%Sn10 wt.%S-AG and 10 wt.%Sn10 wt.%S-MCMB composites are shown in Figure 7(a) and Figure 7(b), respectively. The SEM images of the 20 wt.%Sn20 wt.%S-AG and 20 wt.%Sn20 wt.%S-MCMB composites are shown in Figure 7(c) and Figure 7(d), respectively. It can be seen that all the SnS particles appear to have a flower-like shape. This flower-like shape of SnS was previously observed by Wen Cai *et al.* [21]. The formation of this unique structure was explained using thiourea as a sulfide

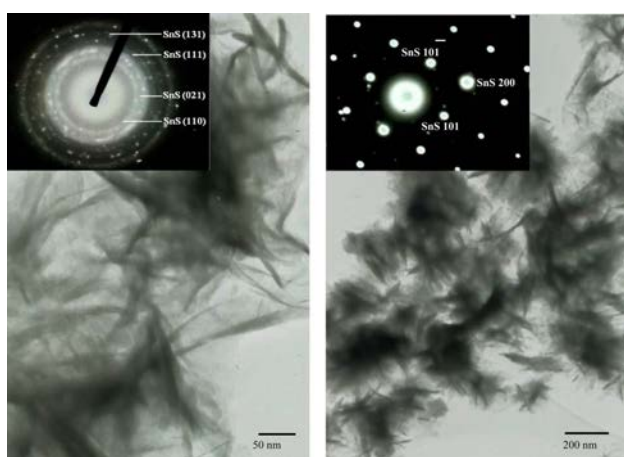


Fig. 8. The TEM images of (a) 10 Sn10 S/Carbon composite and (b) 20 Sn20 S/Carbon composite.

source, which dissolved in *N,N*-dimethylformamide (DMF). It was found that DMF facilitated the formation of the SnS microflowers [21]. However, ethylene glycol, which was used in the present process as the solvent, may also have been of help in the formation of particles with a flower-like shape, with nanodimensions.

Figure 8(a) shows the TEM images of the 10 wt.%Sn10wt.%S-C particles that have a flower-like shape, and Figure 8(b) shows the TEM images of the 20 wt.%Sn20 wt.%S-C. The morphologies observed by the TEM images in all the samples were well consistent with the SEM results. The SAD patterns of the SnS/C show that this sample contained the phases which corresponded to carbon (JCPDS card no. 41-1487) and SnS (JCPDS card no. 39-354), an observation that is well consistent with the XRD results. Moreover, the corresponding SAD patterns of SnS/C reveal that it is a single crystal.

In summary, it can be stated that Sn and SnS on carbon (Sn/C and SnS/C) were successfully prepared using the solution method, which is one of the methods used to obtain nano-scale materials. The solution method is considered simple and low cost. The phases and morphology of all the materials were studied by the XRD, SEM, and TEM techniques. The Sn particles were spherical in shape, and they were well distributed on the surface of the carbon. On the other hand, the shape of the SnS/C composites was flower-like. The smallest particle size was obtained for the Sn on GC sample which used graphene, and it is expected that such composites will have smaller volume changes during the lithium intercalation reaction.

Conclusions

Preparation of Sn and SnS on carbon (Sn/C and SnS/C) was achieved via chemical method for use as anode materials in lithium-ion batteries. All the samples of the Sn/C composites contained the phases, which

corresponded to carbon and Sn. The EDS and the TGA results indicate that there are slight elemental amount deficiencies in all the composites. The Sn particles are spherical in shape and have nanometer dimensions, and the SnS/C composites have a flower-like shape. Furthermore, the particle sizes of Sn on each carbon type reveal that Sn on GC has the smallest particle size, followed by AG and MCMB, respectively. It was shown that the surface area of the carbon significantly affects the particle size, since AG and MCMB, which have low surface areas, caused the formation of larger Sn particles, while graphene, which has a high surface area, allowed for smaller particles.

Acknowledgments

The authors would like to thank immensely the Center for Innovation in Chemistry (PERCH-CIC), National Research University Project of Thailand (NRU) under Thailand's Office of the Higher Education Commission, Department of Chemistry, Chiang Mai University, and all the members of the Renewable Energy Laboratory for their support.

References

1. L. Balan, R. Schneider, J. Ghanbaja, P. Willmann, D. Billaud, *Electrochim Acta*. 51(17) (2006) 3390-3385.
2. J. Kim, C. Kim, D. Son, M. Choi, B. Park, *J. Power Sources*. 167(2) (2007) 535-529.
3. P. Sobrova, M. Ryvolova, D. Huska, J. Hubalek, I. Provaznik, V. Adam, *J. Electrochem. Sci.* 7(1) (2012) 12-1.
4. T. Momma, N. Shiraiishi, A. Yoshizawa, T. Osaka, A. Gedanken, J. Zhu, L. Sominski, *J. Power Sources*. 97-98 (2012) 200-198.
5. H. Mukaibo, A. Yoshizawa, T. Momma, T. Osaka, *J. Power Sources*. 119-121 (2003) 63-60.
6. K. E. Aifantis, M. Haycock, P. Sanders, S. A. Hackney, *Materials Science and Engineering: A* 529 (2011) 61-55.
7. K. Adpakpang, T. Sarakonsri, K. E. Aifantis, S. A. Hackney, *Rev. Adv. Mater. Sci* 32 (2012) 18-12.
8. G. Park, N. Gunawardhana, H. Nakamura, Y. S. Lee, M. Yoshio, *J. Power Sources* 199 (2012) 299-293.
9. J. Z. Wang, L. Lu, M. Choucair, J. A. Stride, X. Xu, H. K. Liu, *J. Power Sources* 196 (2011) 7034-7030.
10. Y. Yan, Y. X. Yin, S. Xin, J. Su, Y. G. Guo, L. J. Wan, *Electrochim Acta* 91 (2013) 61-58.
11. G. X. Wang, J. Yao, H. K. Liu, S. X. Dou, J. H. Ahn, *Electrochim Acta* 50(2-3) (2004) 522-517.
12. S. Yang, H. Song, X. Chen, *J. Power Sources* 173(1) 2007 494-487.
13. S. Yang, H. Song, H. Yi, W. Liu, H. Zhang, X. Chen, *Electrochim Acta* 55(2) (2009) 527-521.
14. Y. Zhang, X. G. Zhang, H. L. Zhang, Z. G. Zhao, F. Li, C. Liu, H. M. Cheng, *Electrochim Acta* 2006 51(23) 5000-4994.
15. S. Liang, X. Zhu, P. Lian, W. Yang, H. Wang, *J. SOLID STATE CHEM* 184(6) (2011) 1404-1400.
16. M. Z. Kassae, E. Motamedi, M. Majdi, *Chemical Engineering Journal* 172(1) (2011) 549-540.
17. S. Kaowphong, P. Thavornnyutikarn. In "Inorganic Chemistry Laboratory" Chiang Mai University, Thailand; 2012.

18. V. Singh, D. Joung, L. Zhai, S. Das, S. I. Khondaker, S. Seal, *PROG MATER SCI* 56(8) (2011) 1271-1178.
19. C. Suryanarayana, M. Grant Norton. In "X-Ray Diffraction: A Practical Approach". New York and London; 1988.
20. W. J. Zhang, *J. Power Sources* 196(13) (2011) 5385-5377.
21. P. Kun, F. Wéber, C. Balázs, *Cent.Eur.J.Chem* 9(1) (2011) 51-47.
22. W. Cai, J. Hu, T. Zhao, H. Yang, J. Wang, W. Xiang, *ADV POWDER TECHNOL* 23(6) (2012) 854-850.